Coherence scanning in a geometrically-desensitized interferometer

Leslie Deck, Peter de Groot, and Xavier Colonna de Lega
Zygo Corporation
Laurel Brook Road, Middlefield, CT. 06455-0448

ABSTRACT

A geometrically desensitized interferometer (GDI) uses two beams incident on the same sample area at different angles of incidence to generate an interference pattern with an equivalent wavelength larger than the illumination wavelength. The instrument is well adapted to the metrology of both smooth and rough samples that are beyond the range of conventional interferometers, while providing more accuracy than conventional moiré techniques.

In this paper, we extend the capabilities of a GDI with an equivalent wavelength of 12.5 microns using coherence scanning in a manner similar to that of scanning white light interferometry. We also present new analysis techniques to accommodate speckle phenomena that can be more prominent in GDI than in white light interferometry. Our scanning GDI can rapidly characterize the surface flatness and relative heights of discontinuous surface features over large measurement volumes.

Key words: Interferometry, phase shifting.

1. INTRODUCTION

The range of surface features and degree of surface quality makes it difficult to provide optical methods for surface metrology for standard industrial machining processes. With surface roughness of order 1μm, phase shifting interferometry (PSI)[1] techniques with IR CO_2 lasers or grazing incidence geometries reduce the interference contrast loss from roughness induced phase variations.

Recently, we introduced another method for increasing the range of applicability of PSI by means of a geometrically desensitized interferometer (GDI).[2,3] A GDI exploits the reduction of the sensitivity along the propagation direction of the phase difference between two beams of light impinging a surface at slightly different angles of incidence. As is shown in Fig.1, two diffraction gratings generate an interference pattern with a large equivalent wavelength that depends primarily on the geometry of illumination. For angles of incidence α and β for the two beams at the test surface, the equivalent wavelength Λ is given by

$$\Lambda = \frac{\lambda}{\cos(\beta) - \cos(\alpha)}. \qquad (1.)$$

Thus a suitable choice of angles can produce an equivalent wavelength of scores or even hundreds of

Part of the SPIE Conference on Three-Dimensional Imaging, Optical Metrology, and Inspection IV
Boston, Massachusetts • November 1998
SPIE Vol. 3520 • 0277-786X/99/$10.00

microns, greatly extending the range of measurable surface features using PSI techniques. However, there are a number of limitations to extending PSI techniques via ever larger equivalent wavelengths in a GDI. Probably the most severe is that as the equivalent wavelength increases to accommodate larger surface discontinuities, the phase extraction resolution remains constant and physical height resolution is sacrificed.

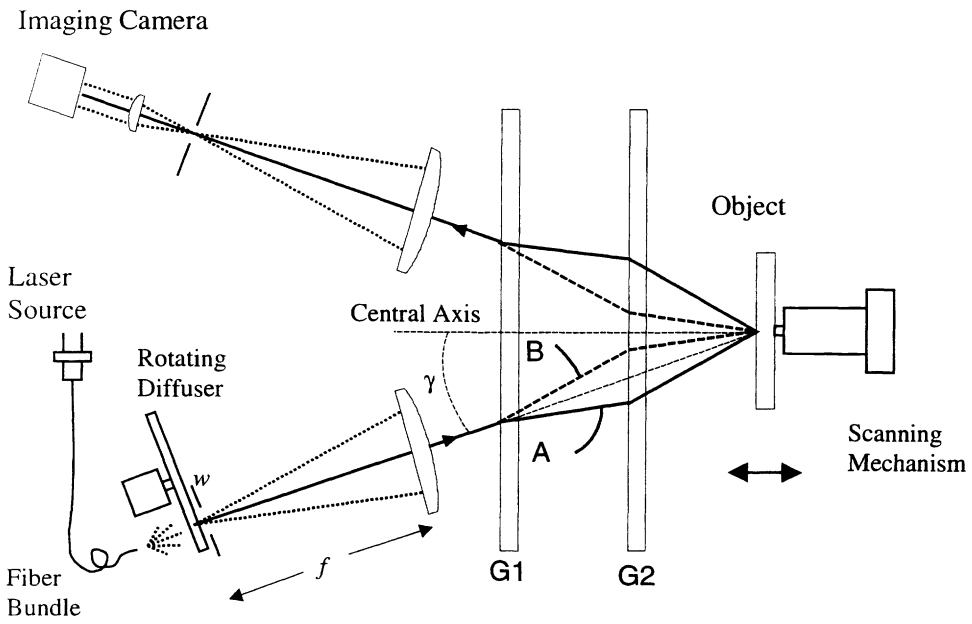

Figure 1: Layout of experimental GDI

A widely-known technique to extend the range of visible wavelength interferometry is coherence scanning.[4,5,6] Increasing the illumination bandwidth in standard visible light interferometry localizes the coherence function about the equal path condition. Scanning the interferometer through this position establishes the absolute surface height for a multitude of points across the object. Though in principle coherence scanning provides a means to profile topographic discontinuities of arbitrary height, rough surfaces such as those produced by conventional machining methods are still difficult to profile with wavelengths over large areas.[7] Typical machining processes produce high lateral frequency surface height variations – referred to as "roughness". When the amplitude of the rough surface exceeds about 1/10 the optical wavelength, phase variations across a sampling element (typically a camera pixel) obliterate the interference contrast.

What is required is a wavelength long compared to the roughness length scale so that phase variations due to roughness are much smaller than 1/10 of the wavelength. Combining the long equivalent wavelength characteristics of GDI systems with coherence scanning techniques offers a new way of profiling an important class of surfaces that have heretofore been mainly ignored by precision optical measurements.[8] This paper presents the use of coherence scanning techniques with one particular dual grating GDI geometry.

2. GDI COHERENCE

A characteristic of dual-grating GDI is that the interference pattern is achromatic, thus unlike standard broad-band interferometry, the fringe spacing is nearly independent of the source wavelength.[2] However, there is an axial variation in fringe contrast associated with the spatial dimensions of the source, consequently adjusting the source size controls the coherence function width. Furthermore, with optically rough surfaces, there is a natural localization of the interference fringe visibility for much the same physical reasons. This feature provides the opportunity to use coherence scanning techniques with GDIs.

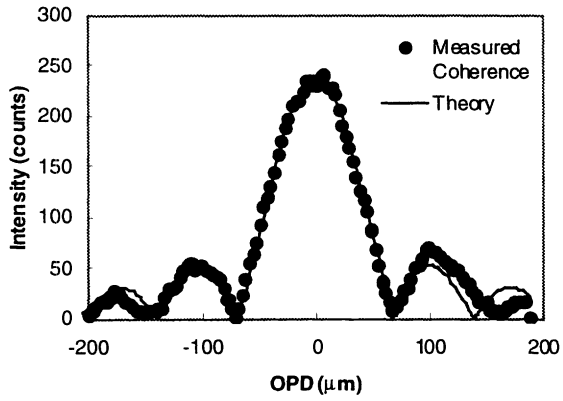

Figure 2: Comparison of measured and theoretical coherence functions.

The grating geometry shown in Figure 1 has a grating frequency of the second grating exactly twice the first, and the spacing between first and second gratings equal to the spacing between the second grating and the test surface. The illumination angle γ is small (9 degrees). Using the grating equation and Eq. 1 in the small angle limit it is easy to show that for this geometry the equivalent wavelength can be written:

$$\Lambda \approx \frac{1}{2N_1\gamma}, \tag{2.}$$

where N_1 is the grating frequency of the first grating. The independence of the equivalent wavelength to the source wavelength is now seen explicitly. The shape of the coherence function V can be derived by integrating the intensity from the single equivalent wavelength 2-beam interference equation over the range of equivalent wavelengths $\Delta\Lambda$ produced by the variation $\Delta\gamma$ in incident angle from points along the source aperture. For a rectangular source aperture, the coherence obeys a sinc function:[9]

$$V = \left| \frac{\sin(z\,\Delta K)}{z\,\Delta K} \right|. \tag{3.}$$

where

$$\Delta K = 2\pi \frac{\Delta\Lambda}{\Lambda^2} \tag{4.}$$

and z is the axial position of the object. The first minimum z_0 of the sinc occurs when its argument is $\pm\pi$:

$$z_0 = \frac{\Lambda^2}{2\Delta\Lambda}. \tag{5.}$$

Taking the coherence width W as the distance between first minima;

$$W = 2z_0 = \frac{\Lambda^2}{\Delta\Lambda} = \left(\frac{1}{2N_1\gamma}\right)^2 \Big/ \frac{\Delta\gamma}{2N_1\gamma^2} = \frac{1}{2N_1\Delta\gamma}. \tag{6.}$$

Thus increasing the range of incident angles decreases the coherence width. The range of angles $\Delta\gamma$ will depend on the focal length of the illumination lens f and the width of the source aperture w via $\Delta\gamma = w/f$. The GDI used for this study had a grating frequency N_1 of 250 cycles/mm, an illumination lens focal length f of 450 mm and two source width options produced by changing the orientation of the fiber bundle illuminator endface. The endface was shaped as a line so by rotating the endface through 90 degrees, the width of the source plane could be changed. A "long" coherence mode orientation provided millimeters of coherence, while the "short" coherence mode orientation, providing a source width w of 6.5mm, produced a coherence width of 138μm. Figure 2 illustrates the excellent agreement between measured and theoretical coherence functions in the short coherence mode.

3. COHERENCE SCANNING

Figure 1 shows the setup for coherence scanning. The test surface is perpendicular to the system central axis and scans along this axis through the equal path condition by means of a precision stepper motor (a Melles Griot Nanomover™) at a speed of 95μm/sec. This results in a 90° phase shift between each frame of the 60Hz imaging camera. The illumination source was a 100mW 680nm multimode laser diode (Philips CQL-802). A personal computer controls the acquisition process.

An Imaging Technology IC-PCI frame-grabber digitizes the camera frames at video rates to 8 bit precision. Computer memory stores the interference patterns so that we can explore various analysis options. Many different analysis techniques are described in the literature.[10,11] Typically they rely on locating the scan position of a contrast feature point (e.g. the peak contrast) for each surface point imaged onto the CCD. This produces a coarse profile for identifying the fringe order. The phase of the interference at the contrast feature point then improves the profile resolution.

4. SMOOTH SURFACES

For strongly reflecting smooth surfaces, the coherence pattern generated during a scan is very clean; however for weakly reflecting smooth surfaces, the coherence pattern exhibits significant distortions. This phenomenon can be traced to the coherence characteristics of the source. For strongly reflecting surfaces the source intensity (determined by the laser diode current) is reduced to prevent camera saturation to a point where the diode was barely lasing and the coherence is very low. For weakly reflecting or rough surfaces the diode current is raised to where most of the energy of the laser is concentrated in a few longitudinal modes. These highly coherent modes together with the extended source produced a speckle pattern that corrupts the interference pattern generated by the surface. Though this "source" speckle pattern varies slowly relative to the interference pattern during a scan, it can still vary significantly over the displacement needed to fully sample the coherence envelope.

To reduce the effect of source speckle noise with smooth surfaces, a rotating diffuser disk can be placed at the source plane. The diffuser rotates at 60Hz so as to average one cycle of the speckle pattern during each camera frame. Figure 3 illustrates the improvement with the rotating diffuser for a polished glass surface (4% reflective). Measurements of polished glass surfaces using coherence scanning techniques with a 12.5μm equivalent wavelength achieved an rms repeatability of 24nm. Figure 4 shows a coherence scanning measurement of a 13.4μm step standard. The system measured the step height at 13.19μm – within 1.5% of the accepted value, with a repeatability of 40nm and a reproducibility (remove and replace part) of better than 200nm.

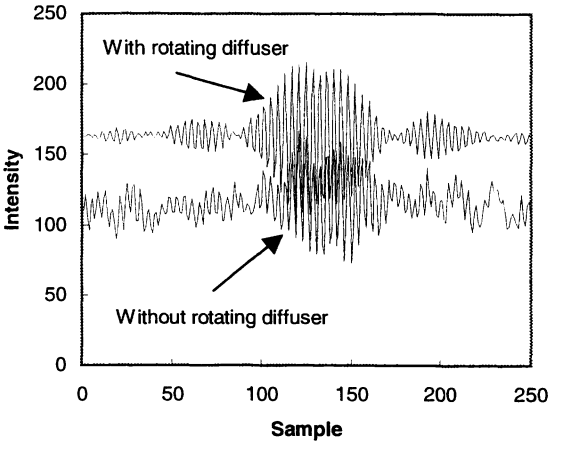

Figure 3: Comparison of interference signals from a smooth low reflectivity part showing improvement when a rotating diffuser is used to average out source speckle.

5. ROUGH SURFACES

Though the influence of the source speckle pattern variation can be effectively removed using a rotating diffuser, another speckle pattern, this time due to the roughness of the test surface coupled with the imaging system numerical aperture, is more difficult to contend with.

In the imaging leg of the GDI system each point on the test surface acts as a source point that is focused onto the camera with a resolution defined by the imaging system point spread function (PSF). For rough objects, rays emanating from neighboring points have a random distribution of phases associated with the random variations of surface heights, so the complex amplitude at a point in the image plane will be proportional to the vector sum of the amplitudes from source points whose PSFs overlap. This summing of random phases leads to speckle that is correlated in a rather complicated way with the test surface profile. This "object" speckle is not removed by the rotating diffuser and depends only on the object roughness and the imaging system numerical aperture.

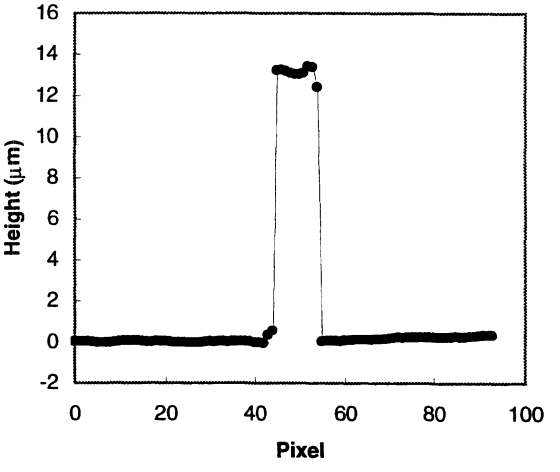

Figure 4: Coherence scanning measurement of a 13.4μm step standard.

There are in fact two speckle fields generated by reflection from the test surface, one for each angle of incidence, which propagate slightly differently back to the imager. Since the speckle fields are generated from the same surface, they correlate maximally at the position of best focus. In the current setup, the plane of zero OPD defined by the short coherence mode is parallel to, but not coextensive with, the plane of best focus. For extremely rough surfaces we use the long source coherence mode for which the best fringe contrast position is at the best focus position. This conveniently is the position for which the system accuracy is optimized.[12]

An example of a rough surface of commercial interest is an aluminum hard disk blank. These blanks have a typical roughness of order 500nm rms, making it impossible to obtain fringes with visible wavelengths. The roughness of this part is severe enough to produce problems even with an equivalent

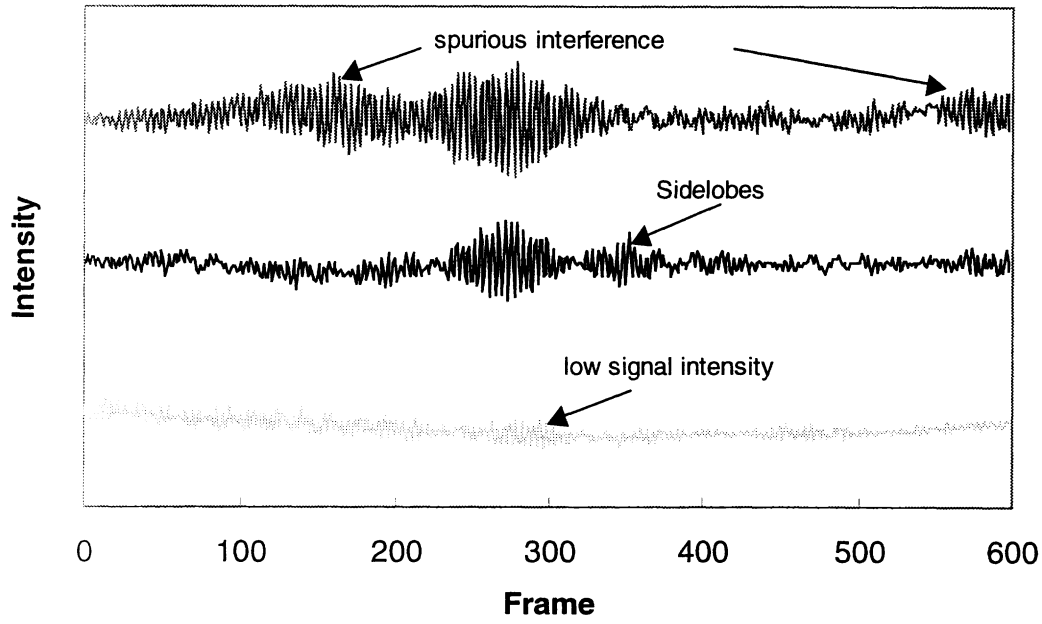

Figure 5: Coherence functions from a rough surface illustrating typical problems encountered, including low signal intensity and spurious interference. The signals have been vertically offset for clarity.

wavelength of 12.5μm. Figure 5 shows the coherence functions obtained from various pixels during a measurement of a hard disk blank. A number of problems occur, including loss of interference and the appearance of additional interference regions far removed from the main coherence peak. These problems make it difficult to accurately determine the fringe order on an individual pixel basis, leading to phase measurement errors of a multiple of 2π for those pixels that exhibit these problems. These "2π discontinuities" produce spurious peaks in the height profile whose deviation from the local surface mean is a multiple of a fringe length – 6.5μm in our case. This affect can be seen in Figure 6, a line profile of a region of a hard disk blank measured using coherence scanning. This profile predicts a roughness of 6.7μm, much higher than measured with other methods. Close examination of Figure 6 reveals that the data spikes come in fixed steps of one fringe length. These 2π discontinuities are an artifact of assuming that the fringe order measurement for each pixel is error free. If the surface form variation is less than one fringe, the average of all the pixels in a flat region can be used to determine the fringe order for that region, with a corresponding statistical reduction in the error. The result of performing this analysis is shown in Fig. 7. The rms roughness calculated from Fig. 7 is now 420nm, in good agreement with alternative measurements of the surface characteristics. Even though the individual pixel fringe order determination is corrupted by

the test surface speckle pattern, the phase determination is relatively unaffected. There may be two reasons for this. First, speckle intensity variations are reduced since a number of speckles are integrated at each detector element. This is seen from the ratio of the area of the imaging element to the area of a speckle at the image.

$$R = \frac{D_{\text{pixel}}^{\ 2}}{D_{\text{speckle}}^{\ 2}} \approx D_{\text{pixel}}^{\ 2} \Big/ \left(\frac{2.4\lambda}{\text{NA}}\right)^2 \approx 4 \qquad (7.)$$

where NA is the imaging numerical aperture. Secondly, because the difference between the two incident angles is small, the speckle decorrelation function can be expected to vary slowly compared to the interference frequency. The spectral regime used to extract the phase is thus far removed from the source of the corruption. The analysis methodology for very rough surfaces then becomes one of first determining the flat regions using the position of the coherence feature, calculating for that region a fringe order surface variation from all the data in the region and to use this fringe order surface as a starting point for the individual pixel phase determination.

For surfaces with moderate roughness, (less than 100nm rms in our case) the speckle fields formed by the reflection of the two angled plane waves A and B in Figure 1 correlate well in the image plane. This assures a well developed coherence function with a single strong peak. The fringe order at the chosen coherence feature is then easily identified with good signal to noise. Profiles from these surfaces easily obtained and highly repeatable. Figure 8 shows the line profile across two abutting gauge blocks (130 and 150 mil) each with an rms roughness of about 60nm. The step height, measured to be 517 μm, was very close to the expected value of 20mil = 508μm.

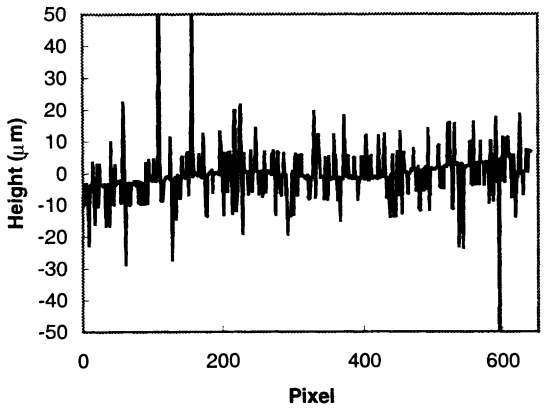

Figure 6: Line profile of a rough surface using individual fringe order determination.

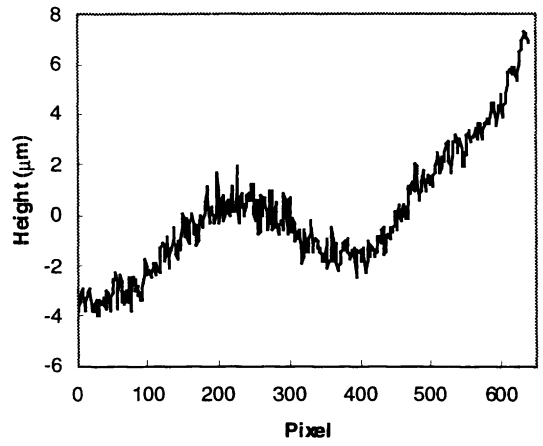

Figure 7: Profile of a rough surface using the average of many pixels to calculate the fringe order.

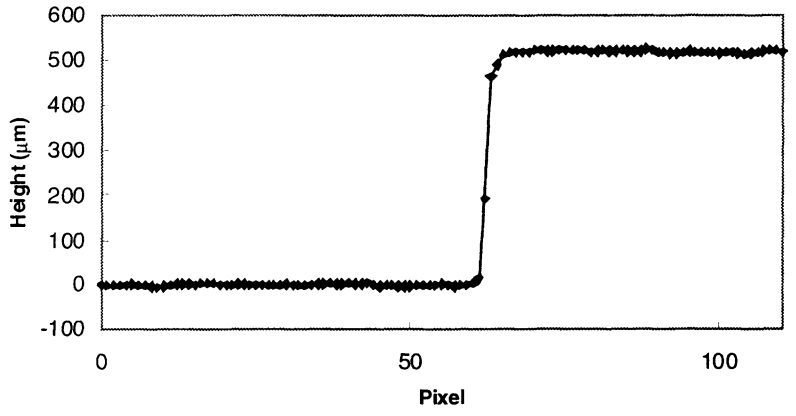

Figure 8: Line profile across 130 and 150 mil abutting gauge blocks.

6. SUMMARY

We have shown that coherence scanning greatly extends the measurement capabilities of a GDI. In developing the technique, we have found that it is important to introduce a rotating glass diffuser in the source light and to employ noise-resistant data analyses. The combination of coherence scanning with the long equivalent wavelength characteristics of a GDI system provides the capability to perform topographical measurements of extremely rough flat surface regions with almost unlimited physical departure. In particular we have shown here that the combination can accurately profile surfaces with a roughness typical of standard machining processes.

7. REFERENCES

[1] J. E. Greivenkamp and J. H. Bruning, "Phase Shifting Interferometry", Chap. 14, of "Optical Shop Testing", 2nd Ed., J. Wiley pub, edited by D. Malacara.

[2] P. de Groot, "Grating interferometer for flatness testing," Opt. Lett. 21(3) 228-230 (1996).

[3] Zygo Corporation manufactures a GDI instrument for industrial and data storage markets under the product name MESA. US Pat. Nos. 5,526,116; 5,671,050.

[4] U S Pat. #4,340,306 to N. Balasubramanian

[5] T. Dresel, G. Haeusler and H. Venzke, "Three-dimensional sensing of rough surfaces by coherence radar," Applied Optics 31(7), 919-925 (1992).

[6] L. Deck and P. de Groot, "High-speed non-contact profiler based on scanning white light interferometry," Appl. Opt. 33(31), 7334-7338 (1995).

[7] J. Roth and P. de Groot, " Wide-field scanning white light interferometry of rough surfaces," Proc. ASPE Spring Topical Meeting on Advances in Surface Metrology, p.57-60 (1997).

[8] US Patent No. 5,598,265 to P. de Groot

[9] P. de Groot, L. Deck, X. Colonna de Lega, "Adjustable coherence depth in a geometrically-desensitized interferometer," Proc. SPIE, 3479, 14-23 (1998)

[10] US Pat. No. 5,471,303 to C. Ai and P. Caber

[11] US Pat. No. 5,398,113 to P. de Groot

[12] X. Colonna de Lega, J. Biegen, D. Stephenson, P. de Groot, "Characterization of a geometrically desensitized interferometer for flatness testing," Proc. SPIE, 3520, (1998)